

図 2. (a) 宇都宮，東京，銚子，前橋の気象庁観測点における（左）S-P 時間，（右）初動（赤；上方動，青；下方動）を気象庁カタログ（1923 年 1 月 14 日～2011 年 12 月 31 日）の震央にプロットしたもの．星印はそれぞれの観測点の位置を表す．(b) 柏（E.KW8M），本郷（E.YYIM; 弥生（東京大学地震研究所構内）），横須賀（E.KH2M；第二海堡）ならびに鎌倉震研（E.SYOM）における（左）S-P 時間，（右）初動（赤；上方動，青；下方動）の分布を MeSO-net 検測値から決定した震央（2008 年 4 月 1 日～2014 年 7 月 10 日）にプロットしたもの．

Fig. 2. (a) For each of four stations, Utsunomiya, Tokyo, Choshi, and Maebashi, observed S-P times (left) and first-motion polarities (right) are plotted at epicenters of the JMA catalog from January 14th, 1923 to December 31st, 2011. White star indicates the location of each observation station. (b) For each of four stations, Kashiwa (E.KW8M), Hongo (E.YYIM; Yayoi), Yokosuka (E.KH2M), and Kamakura (E.SYOM), observed S-P times (left) and first-motion polarities (right) are plotted at epicenters determined by using pick data from MeSO-net and other networks from April 1st, 2008 to July 10th, 2014. White star indicates the location of each observation station.

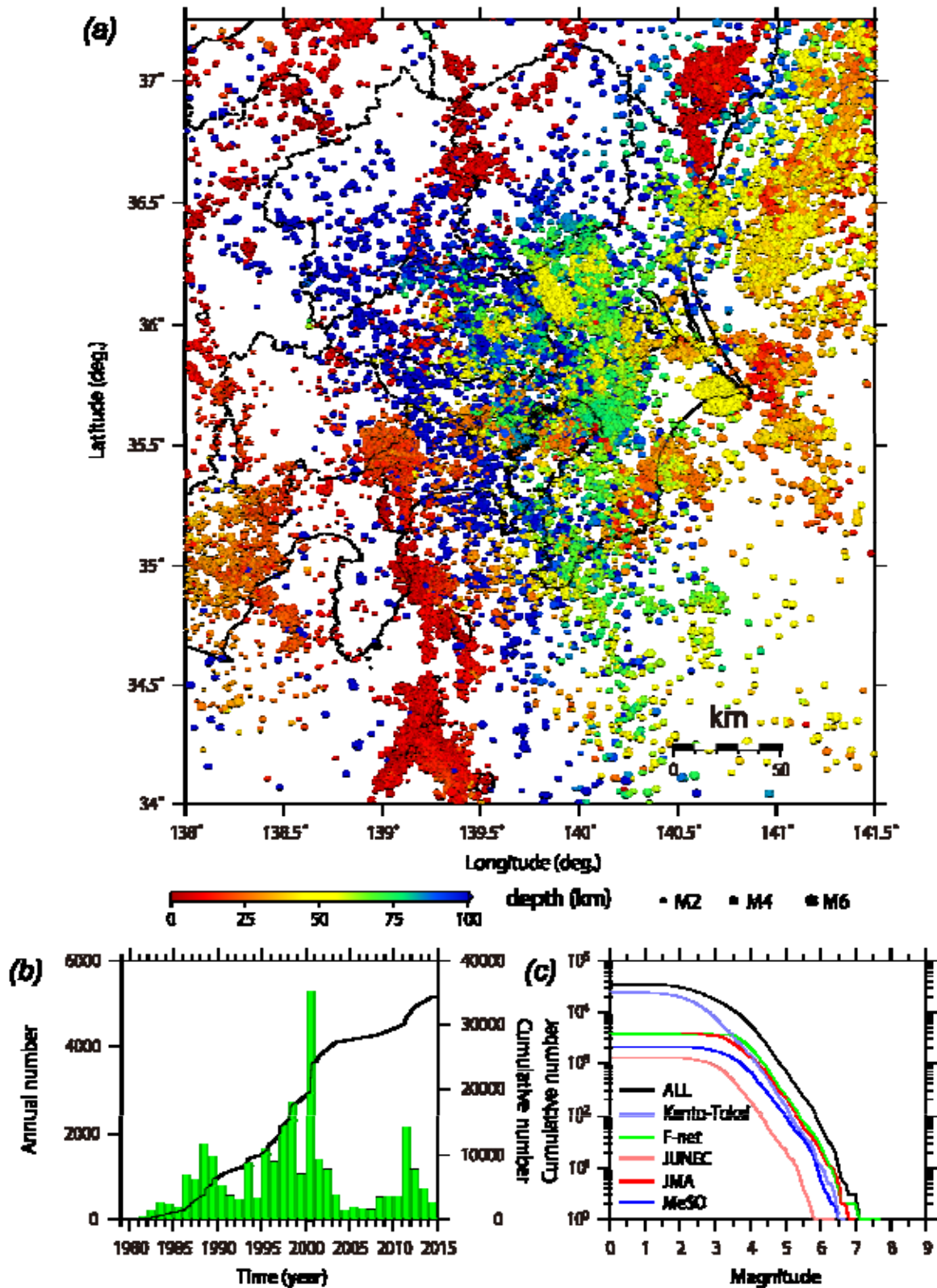


図 4. (a) 関東ならびにその周辺域において5つのカタログから整理された発震機構解をもつ地震の震央分布. 色は震源の深さを表す. (b) 1年あたりの発震機構解数(棒グラフ; 左軸)ならびに累積頻度曲線(実線; 右軸). (c) 本研究で整理した発震機構解が推定された地震の規模別頻度分布.

Fig. 4. (a) Distribution of earthquakes for which focal mechanism solutions were compiled from five catalogs. The colors indicate hypocentral depths. (b) Annual frequency of earthquakes with compiled focal mechanisms (green bars; left axis) and cumulative frequency curve (black line; right axis). (c) Magnitude-frequency distribution of earthquakes that the focal mechanism solutions were compiled.

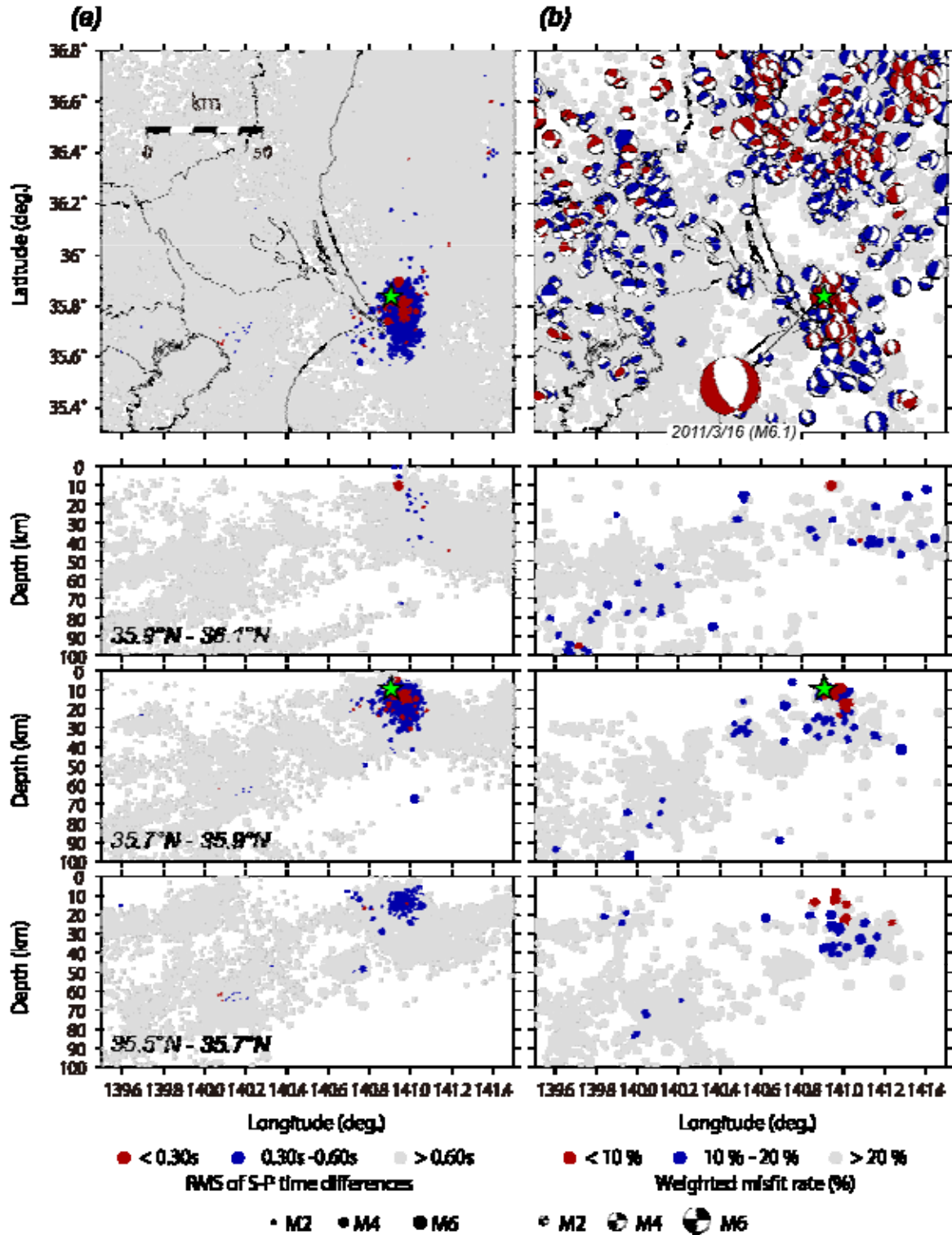


図 5. (a) 2011 年 3 月 16 日の地震 ($M6.1$) と近年の地震との間の S-P 時間の残差の二乗平均平方根の分布ならびにその東西断面図. 緑星印は気象庁による震源を表す. (b) 近年の地震の発震機構解に対する重み付きミスフィット率の分布ならびにその東西断面図. 重み付きミスフィット率が 20% 以下の発震機構解のみを震源球表示している.

Fig. 5. (a) Distribution of root mean squares of S-P time differences between recent earthquakes and the earthquake of March 16th, 2011. East-west cross sections for $35.9^{\circ}\text{N}-36.1^{\circ}\text{N}$, $35.7^{\circ}\text{N}-35.9^{\circ}\text{N}$, and $35.5^{\circ}\text{N}-35.7^{\circ}\text{N}$ are also shown. Green star indicates the hypocenter of earthquake on March 16th, 2011 by JMA. (b) Distribution of weighted misfit rates of the first-motion polarities reported for the earthquake of March 16th, 2011 for focal mechanism solutions for recent earthquakes. Only focal mechanism solutions with weighted misfit rates $\leq 20\%$ are shown in the lower hemispheres. East-west cross sections for $35.9^{\circ}\text{N}-36.1^{\circ}\text{N}$, $35.7^{\circ}\text{N}-35.9^{\circ}\text{N}$, and $35.5^{\circ}\text{N}-35.7^{\circ}\text{N}$ are also shown.

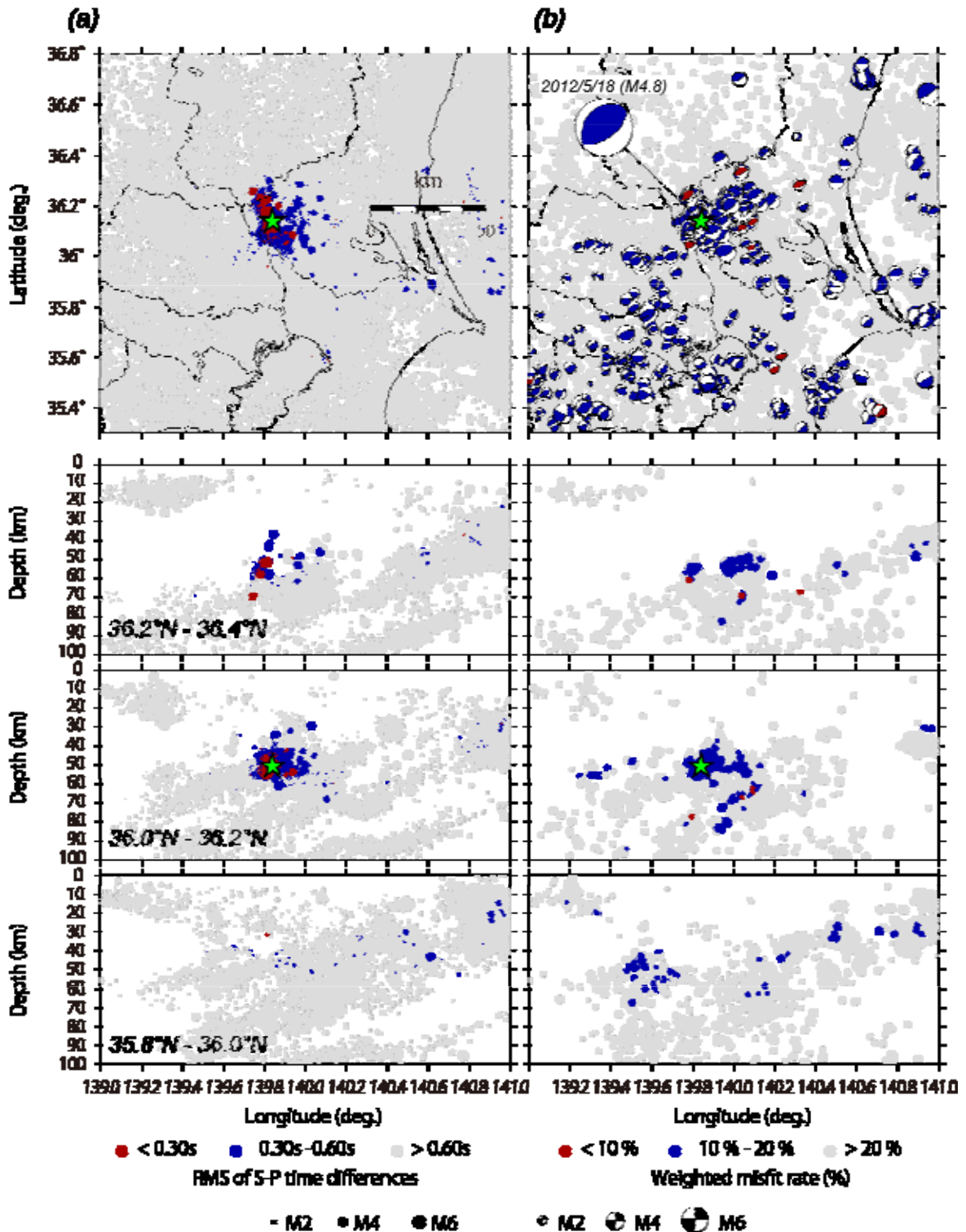


図 6. (a) 2012 年 5 月 18 日の地震 (M4.8) と近年の地震との間の S-P 時間の残差の二乗平均平方根の分布ならびにその東西断面図. 緑星印は気象庁による震源を表す. (b) 近年の地震の発震機構解に対する重み付きミスフィット率の分布ならびにその東西断面図. 重み付きミスフィット率が 20% 以下の発震機構解のみを震源球表示している.

Fig. 6. (a) Distribution of root mean squares of S-P time differences between recent earthquakes and the earthquake of May 18th, 2012. Green star indicates the hypocenter of earthquake on May 18th, 2012 by JMA. East-west cross sections for 36.2°-36.4°N, 36.0°-36.2°N, and 35.8°-36.0°N are also shown. (b) Distribution of weighted misfit rates of the first-motion polarities reported for the earthquake of May 18th, 2012 for focal mechanism solutions for recent earthquakes. Only focal mechanism solutions with weighted misfit rates $\leq 20\%$ are shown in the lower hemispheres. East-west cross sections for 36.2°-36.4°N, 36.0°-36.2°N, and 35.8°-36.0°N are also shown.

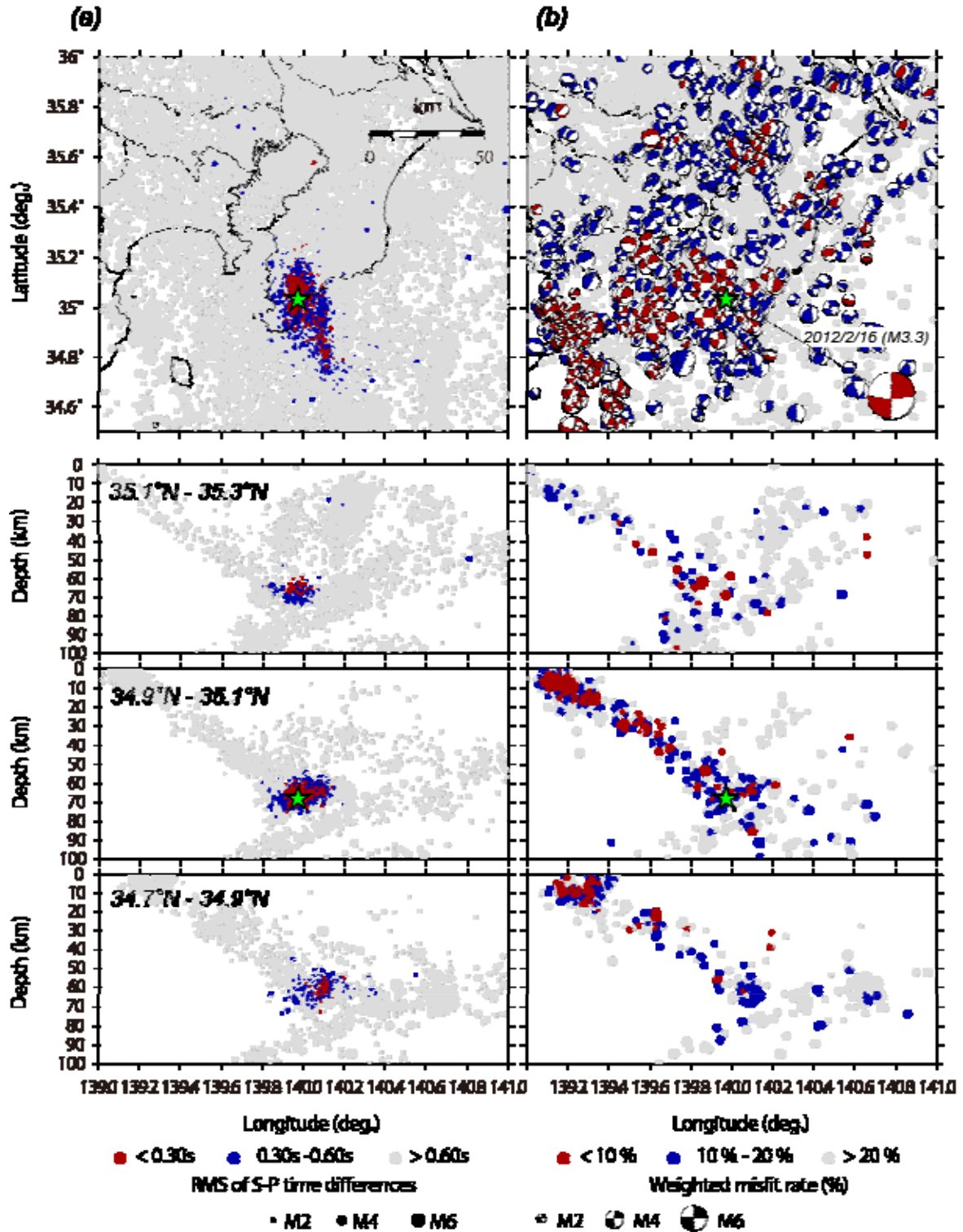


図 7. (a) 2012 年 2 月 16 日の地震 (M3.3) と近年の地震との間の S-P 時間の残差の二乗平均平方根の分布ならびにその東西断面図。緑星印は気象庁による震源を表す。(b) 近年の地震の発震機構解に対する重み付きミスフィット率の分布ならびにその東西断面図。重み付きミスフィット率が 20% 以下の発震機構解のみを震源球表示している。

Fig. 7. (a) Distribution of root mean squares of S-P time differences between recent earthquakes and the earthquake of February 16th, 2012. East-west cross sections for 35.1°-35.3°N, 34.9°-35.1°N, and 34.7°-34.9°N are also shown. Green star indicates the hypocenter of earthquake on February 16th, 2012 by JMA. (b) Distribution of weighted misfit rates of the first-motion polarities reported for the earthquake of February 16th, 2012 for focal mechanism solutions of recent earthquakes. Only focal mechanism solutions with weighted misfit rates $\leq 20\%$ are shown in the lower hemispheres. East-west cross sections for 35.1°-35.3°N, 34.9°-35.1°N, and 34.7°-34.9°N are also shown.

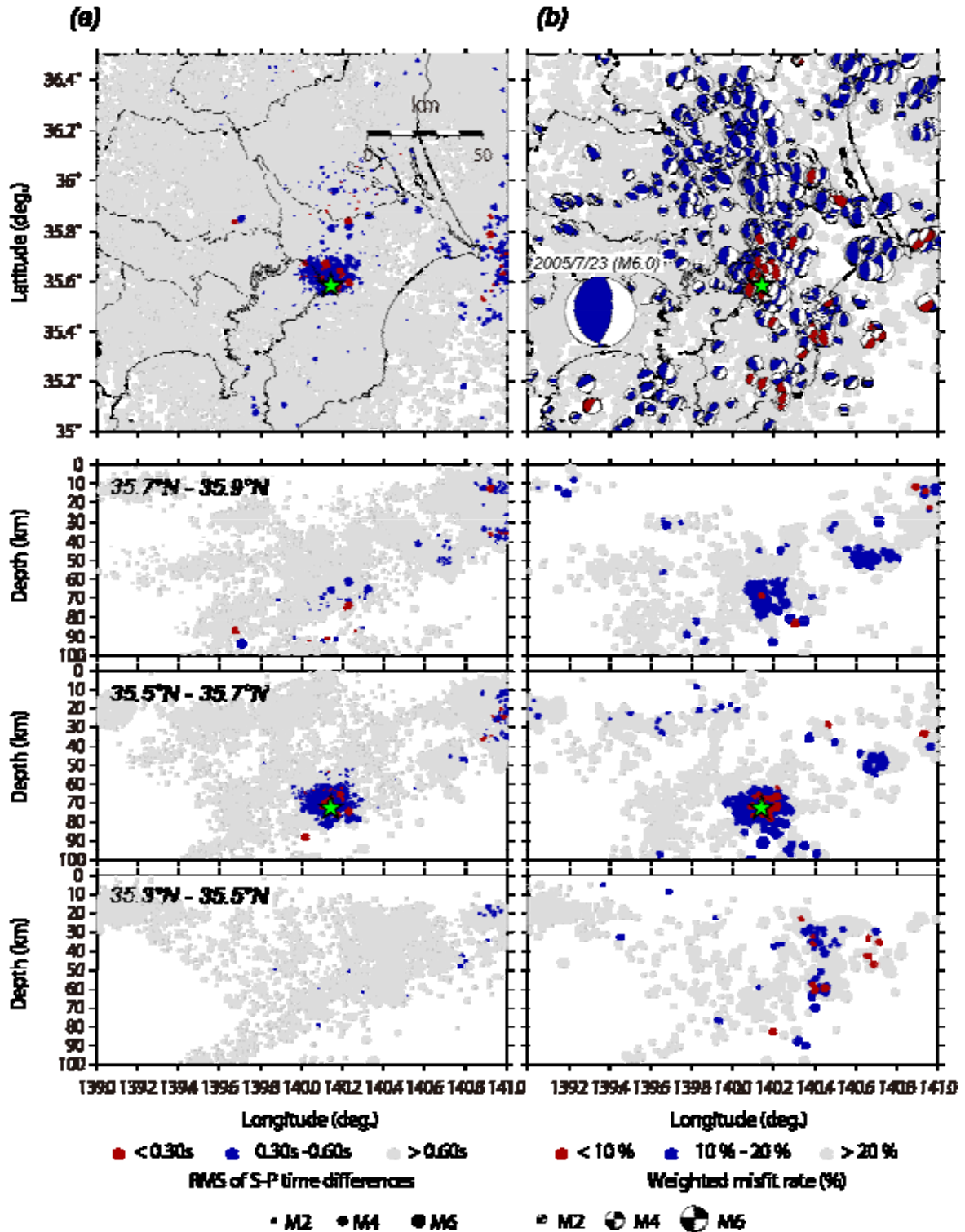


図 8 . (a) 2005 年 7 月 23 日の地震 ($M6.0$) と近年の地震との間の S-P 時間の残差の二乗平均平方根の分布ならびにその東西断面図 . 緑星印は気象庁による震源を表す . (b) 近年の地震の発震機構解に対する重み付きミスフィット率の分布ならびにその東西断面図 . 重み付きミスフィット率が 20% 以下の発震機構解のみを震源球表示している .

Fig. 8. (a) Distribution of root mean squares of S-P time differences between recent earthquakes and the earthquake of July 23th, 2005. East-west cross sections for 35.7° - 35.9° N, 35.5° - 35.7° N, and 35.3° - 35.5° N are also shown. Green star indicates the hypocenter of earthquake on July 23th, 2005 by JMA. (b) Distribution of weighted misfit rates of the first-motion polarities reported for the earthquake of July 23th, 2005 for focal mechanism solutions for recent earthquakes. Only focal mechanism solutions with weighted misfit rates $\leq 20\%$ are shown in the lower hemispheres. East-west cross sections for 35.7° - 35.9° N, 35.5° - 35.7° N, and 35.3° - 35.5° N are also shown.

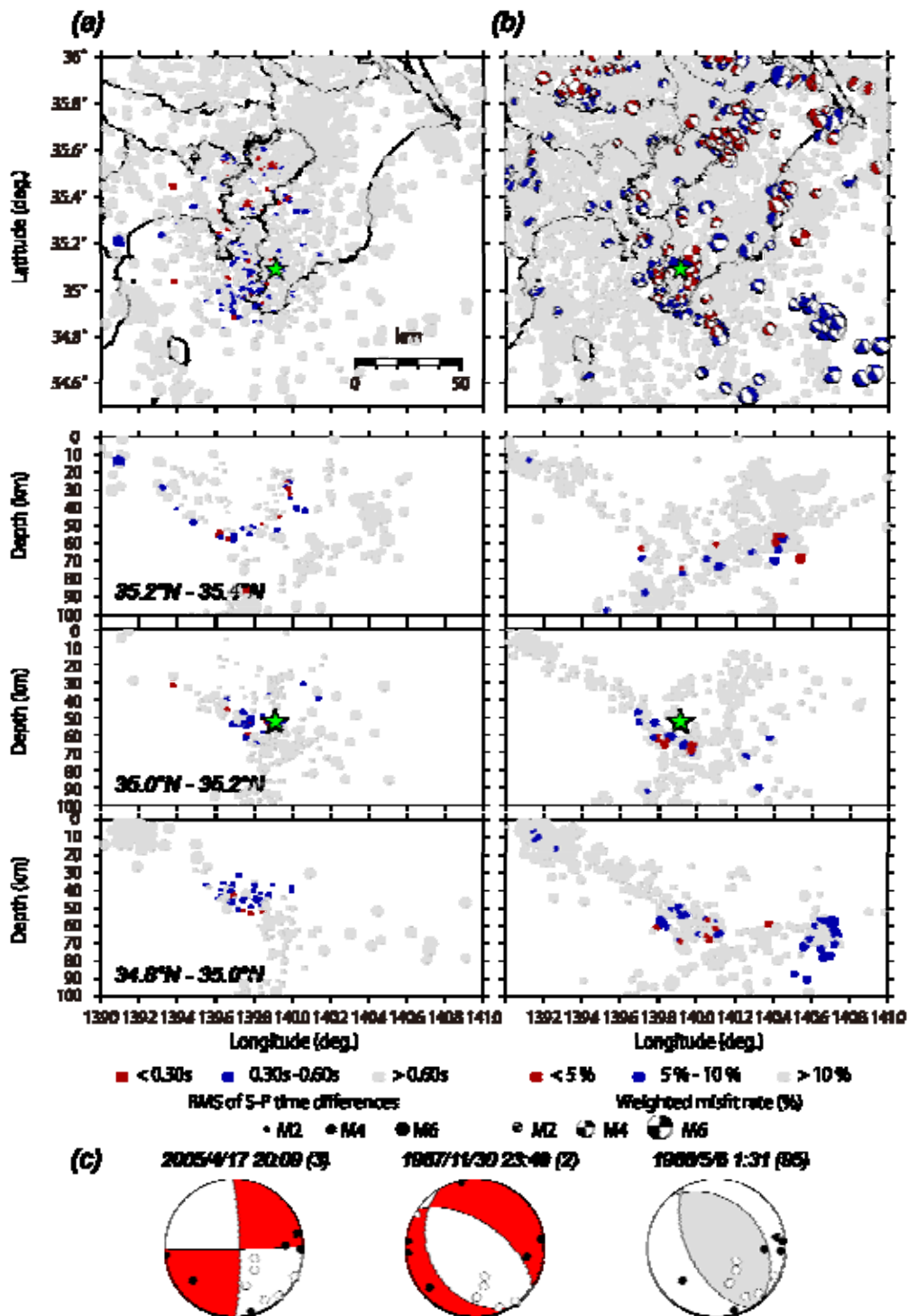


図 10. (a) 1922 年浦賀水道付近の地震と近年の地震との間の S-P 時間の残差の二乗平均平方根の分布ならびにその東西断面図. 緑星印は石辺・他(2012)による 1922 年の地震の震源. (b) 近年の地震の発震機構解に対する重み付きミスフィット率の分布ならびにその東西断面図. 重み付きミスフィット率が 10% 以下の発震機構解のみを震源球表示している. (c) 浦賀水道付近から千葉県南西部に至る領域において発生した 3 地震に対する発震機構解と 1922 年浦賀水道付近の地震に対する初動の分布. 黒丸・白丸はそれぞれ初動が押し・引きを表す. 括弧内の数字は重み付きミスフィット率 (%) を示す.

Fig. 10. (a) Distribution of root mean squares of S-P time differences between recent earthquakes and the 1922 earthquake. East-west cross sections for 35.2°-35.4°N, 35.0°-35.2°N, and 34.8°-35.0°N are also shown. Green star indicates the hypocenter of the 1922 earthquake estimated by Ishibe *et al.* (2012). (b) Distribution of weighted misfit rates of the 1922 first-motion polarities for focal mechanism solutions for recent earthquakes. Only focal mechanism solutions with weighted misfit rates $\leq 10\%$ are shown in the lower hemispheres. (c) The distribution of first-motion polarities (solid circles, push upward; open circles, pull downward) reported for the 1922 earthquake for three focal mechanism solutions of earthquakes. The colors in the expansion of the lower hemisphere indicate the weighted misfit rates as shown in the parenthetical numbers.

口絵 8. 石辺・他 図 11(本文 p.123)

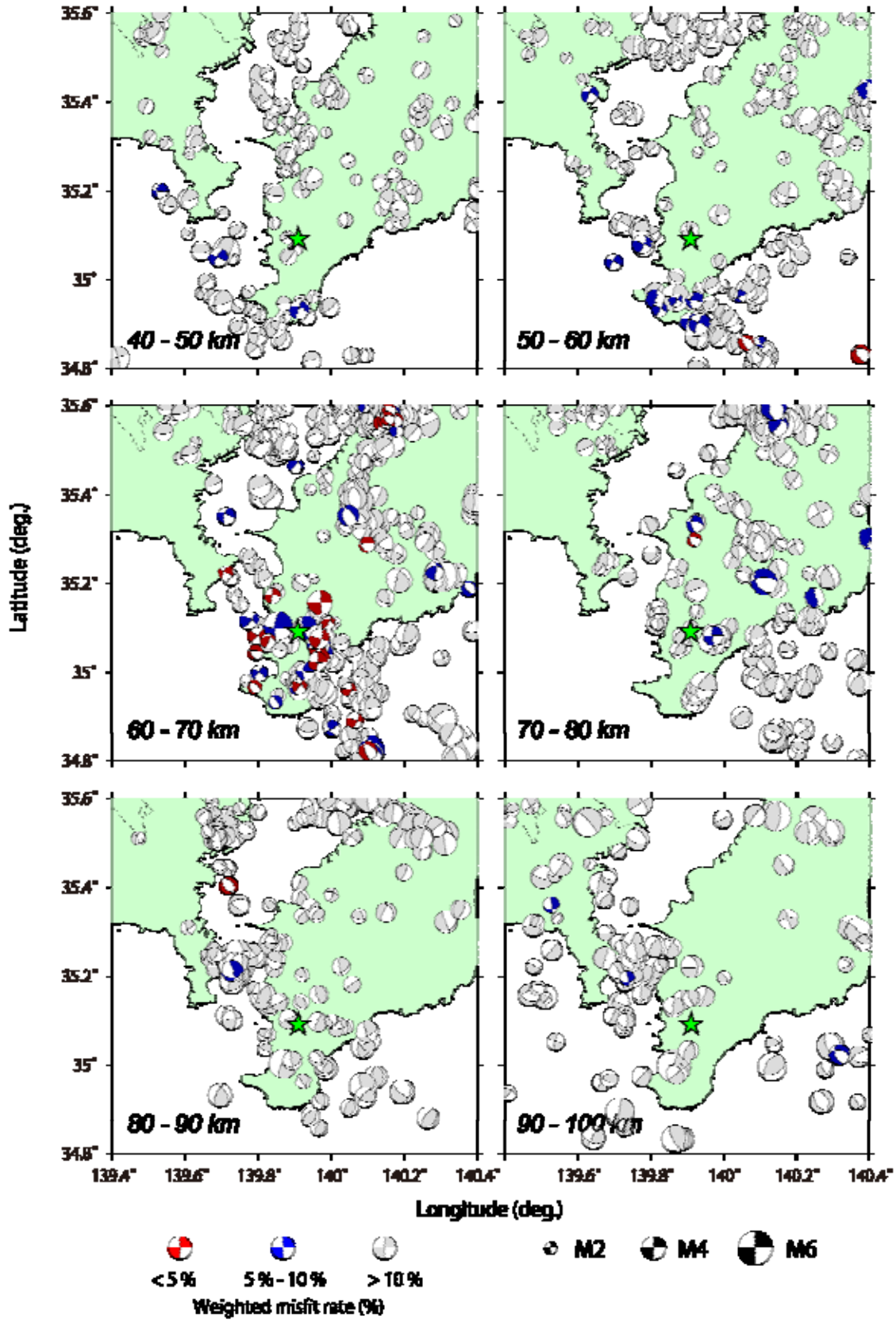


図 11. 1922 年浦賀水道付近の地震に対する初動を用いた近年の地震の発震機構解に対する重み付きミスフィット率の深さ毎の分布. 緑星印は石辺・他(2012)による 1922 年の地震の震央.

Fig. 11. Distribution of weighted misfit rates of the 1922 first-motion polarities for focal mechanism solutions for recent earthquakes for different depths. Green star indicates the epicenter of the 1922 earthquake estimated by Ishibe *et al.* (2012).

